BK_{Ca} nitrosylation is associated with cerebral microvascular dysfunction in female *5x-FAD* mice

Josiane F. Silva[1], Felipe D. Polk[1], Andrea Savu[1], Allison M. Kath[1], Michael T. Gee[1], Paulo W. Pires[1,2,3,*]

[1]Department of Physiology, [2]Sarver Heart Center, [3]Bio5 Institute, University of Arizona College of Medicine, Tucson, AZ, 85721, USA.

*Corresponding Author

Running title: S-nitrosylated-BK_{Ca} channels impair microvascular function

Address for Correspondence: Paulo W. Pires, Ph.D.

1656 E Mabel St, Room 424

Medical Research Building

Tucson, AZ 85721

PO Box 245051

Phone: +1 (520) 626-8632

Email: ppires@arizona.edu

Keywords: female, cerebral pial arteries, BK_{Ca} channels, iNOS, nitrosylation, cerebral functional hyperemia

Abstract

Cerebral microvascular dysfunction and nitro-oxidative stress are present in patients with Alzheimer's disease (AD) and may contribute to disease progression and severity. Large conductance Ca^{2+}-activated K^+ channels (BK_{Ca}) play an essential role in vasodilatory responses and maintenance of myogenic tone in resistance arteries. BK_{Ca} can be modified in a pro-nitro-oxidative environment, resulting in decreased activity and vascular hyper-contractility, which can compromise cerebral blood flow regulation. We hypothesized that reductions in BK_{Ca} function in cerebral arteries, as a consequence of nitro-oxidative stress, are associated with blunted neurovascular responses in the *5x-FAD* model of AD. Using pressure myography, we observed that posterior communicating arteries (PComA) from 5 months-old female *5x-FAD* mice showed higher spontaneous myogenic tone than wild-type (WT) littermates. Constriction to the BK_{Ca} blocker iberiotoxin (30 nM) was smaller in *5x-FAD* than WT, suggesting lower basal BK_{Ca} activity, which was independent of alterations in intracellular Ca^{2+} transients or BK_{Ca} mRNA expression. These vascular changes were associated with higher levels of oxidative stress in female *5x-FAD* and a higher level of S-nitrosylation in the BK_{Ca} α-subunit. In females, pre-incubation of PComA from *5x-FAD* with the reducing agent DTT (10 μM) rescued iberiotoxin-induced contraction. Female *5x-FAD* mice showed increased expression of iNOS mRNA, lower resting cortical perfusion atop the frontal cortex, and impaired neurovascular coupling responses. No significant differences between male *5x-FAD* and WT were observed for all parameters above. These data suggest that the exacerbation in BK_{Ca} S-nitrosylation contributes to cerebrovascular and neurovascular impairments in female *5x-FAD* mice.

Significance Statement

Cerebral vascular dysfunction is increasingly recognized as a hallmark of Alzheimer's disease and other dementias. Impaired microvascular regulation can lead to deficits in blood flow to the brain. An intrinsic property of the resistance vasculature is to constrict when pressurized (myogenic tone), generating a vasodilatory reserve. Detrimental over-constriction is prevented by vascular feedback mechanisms, including the opening of large-conductance Ca^{2+}-activated K^+ channels (BK_{Ca}). Here, using a combination of molecular biology tools with *ex vivo* and *in vivo* vascular assessments, we show a novel mechanism associated with BK_{Ca} dysfunction in the cerebral microvasculature of female *5x-FAD* mice. We report increased BK_{Ca} S-nitrosylation linked to reduced activity and, consequently, higher basal myogenic tone. These changes were associated with lower perfusion of the frontal cortex and impaired neurovascular reactivity,

suggesting that nitro-oxidative stress is an important mechanism of vascular dysfunction in Alzheimer's disease.

Introduction

Alzheimer's disease (AD) is a neurodegenerative disorder associated with global cognitive decline that affects more than 6 million people in the United States alone (1, 2), and approximately 2/3 of all AD cases are women (1, 3). Alarmingly, it is projected that more than 130 million people will live with AD worldwide by 2050 (1, 3). Despite recent advances in the understanding of AD pathophysiology (presence of Apoε4 gene, cerebral accumulation of amyloid-β peptide, and neurofibrillary tangles), there are no truly efficacious treatments for this disease, and clinical trials failed to demonstrate significant improvements in cognitive function with anti-amyloid-β immunotherapy (4). Thus to develop more effective treatments, we must develop a better understanding of the multifactorial aspects of AD.

One of the hallmarks of AD is cerebral amyloid angiopathy (CAA), or perivascular accumulation of amyloid-β, which is present in more than 80% of all AD patients (5). This accumulation is proposed to induce microvascular fragility, contributing to the development of intracerebral hemorrhages (6), blood-brain-barrier leakiness (7), and blood flow deficits (8). These deficits may be a consequence of microvascular dysfunction, which impairs cerebrovascular reserve and neurovascular coupling (9), a vital process that matches local hyperemia to increased neuronal activity (10). The ability of the cerebral microcirculation to accommodate these second-to-second changes in local perfusion depends on two main phenomena: the extent of myogenic tone (the intrinsic contractile property of vascular smooth muscle cells that stipulates the vasodilatory reserve) and mechanisms underlying vasorelaxation. Notably, both mechanisms are dependent on the membrane potential of smooth muscle cells: depolarization favors constriction, whereas hyperpolarization favors dilation. Thus, regulation of ion flux is paramount for microvascular function, particularly modulation of K^+ permeability, of which the large-conductance Ca^{2+}-activated K^+ channel (BK_{Ca}) is central.

BK_{Ca} are widely expressed channels that play a critical role in regulating arterial tone by conducting hyperpolarizing currents in vascular smooth cells to oppose vasoconstriction (11, 12). The opening of BK_{Ca} channels occurs downstream from localized intracellular Ca^{2+} release from ryanodine receptors located in the sarcoplasmic reticulum (*Ca^{2+} sparks*), which activates BK_{Ca} channels, leading to hyperpolarization and dilation (11, 13). BK_{Ca} channels are composed of two

subunits, a selective pore (BKα) and regulatory (BKβ1) subunits (14). Further, BK_{Ca} undergoes extensive pre- and post-translational modifications (PTM), which affect channel open probability and conductance (15). BK_{Ca} phosphorylation has been well documented (15-17), and generally, PKA and PKG-mediated BK_{Ca} phosphorylation leads to channel activation (18-21), whereas PKC phosphorylation results in inactivation (22). However, other PTM, such as nitrosylation and oxidation, can directly impact channel activity. In some tissues, oxidation increases channel activity (23, 24), whereas, in others, it markedly inhibits BK_{Ca} (25-27). Similarly, nitrosylation of thiol moieties (S-NO) due to an electrophilic attack by peroxynitrite inhibits BK_{Ca} currents (28). Peroxynitrite can be generated in cells after a reaction between nitric oxide (NO) and superoxide (O_2^-) in a pro-oxidative environment (29-31). This environment is commonly associated with pathological conditions, such as AD (32-34). A recent study by Taylor *et al.* (35) showed that BK_{Ca} is impaired in the male APP23 mice, a model of AD; however, it remains unknown if PTMs play a role in this impairment. Therefore, we evaluated the contribution of BK_{Ca} to vascular dysfunction related to AD and the possible involvement of PTMs. We hypothesized that a reduction in BK_{Ca} channel function, resulting from nitro-oxidative PTMs, is responsible for cerebral microvascular dysfunction in *5x-FAD* mice.

Results

Amyloid-β accumulation is higher in female 5x-FAD mice

One of the hallmarks of Alzheimer's disease is the accumulation of amyloid-β peptides in the brain and cerebral microvasculature (36). In this study, *5x-FAD* female mice showed a higher density of amyloid-β plaques in the cortex when compared with male *5x-FAD* (Figures 1A and 1B). No statistically significant differences were observed in the hippocampus (Figures 1A and 1B). Interestingly, we did not observe any significant perivascular amyloid-β accumulation in the parenchymal circulation of male or female *5x-FAD* mice (SI Appendix, Figures S1A, and S1B). We previously showed that pial arteries in this model exhibit extensive amyloid-β accumulation (37). However, in our previous publication, we did not separate the incidence of pial vessel CAA by sex. Thus we reanalyzed those data and observed no sex differences in pial vessel CAA in *5x-FAD* mice (SI Appendix, Figures S1C, and S1D). Given the lack of microvascular intraparenchymal CAA in *5x-FAD*, we performed vascular assessments using pial arteries, particularly arteriole-sized PComA.

Cerebral perfusion deficits in female 5x-FAD

Next, we investigated if there are changes in basal cortical perfusion in *5x-FAD* male and female mice compared to wild-type (WT) littermates. Using laser speckle contrast imaging, we observed that the baseline perfusion of the entire superficial cortex was not different between WT and *5x-FAD* females (Figure 1C, WC: whole cortex**)** or males (Figure 1D**,** WC: whole cortex). However, when analyzing perfusion after separating the cortex in different regions (38), *5x-FAD* females showed a reduction in perfusion to the frontal cortex region compared to WT (Figure 1C). No significant differences were observed in cortical perfusion of male *5x-FAD* mice (Figure 1D). For a diagram of how the different cortical regions were separated, see SI Appendix, Figure S2**.**

PComAs from female 5x-FAD mice have increased myogenic tone

Along with amyloid-β plaque accumulation, microvascular dysfunction is implicated in AD pathophysiology (36). Changes in myogenic tone, the intrinsic contractile property of resistance arteries and arterioles facing circumferential stretch (39), can underlie reductions in blood flow (40, 41). Female *5x-FAD* mice showed an approximately 50% increase in the spontaneous myogenic tone in the PComAs compared to female WT (Figure 1E and 1F). No differences were observed in males (Figures 1I and 1J). To investigate the mechanisms involved in the higher myogenic tone on the PComAs from *5x-FAD* female mice, firstly, we tested the PComA contractile response to a depolarizing stimulus, 60 mM KCl. There was no significant difference between the groups of females (Figure 1G) or males (Figure 1K). These results suggest that the rise in myogenic tone is not explained by a hypercontractile response of the vascular smooth muscle cells to a depolarizing stimulus. Then, we evaluated the participation of endothelial cells in PComA dysfunction. Removal of the endothelium increased myogenic tone in female *5x-FAD* and WT mice, although the increase was larger in WT, to the point that myogenic tone was equalized between strains (Figure 1H). Interestingly, endothelium removal did not affect myogenic tone in the male mice (Figure 1L).

We further characterized the structural and biomechanical properties of PComA from male and female WT vs. *5x-FAD* mice. We observed that, in the *5x-FAD* model at 5-6 months of age, no discernible microvascular remodeling or stiffening is present (SI Appendix, Figures S3 and S4)**.** Since PComA dysfunction is presented in the *5x-FAD* female mice group, the following experiments were performed only on female *5x-FAD* and WT mice to identify the mechanisms involved in this dysfunction.

Reduced BK_{Ca} channel function PComA from 5x-FAD females

BK_{Ca} channel is an important mechanism that provides negative feedback to myogenic constriction (39). Therefore, to test that, we incubated PComA with the BK_{Ca} channel blocker iberiotoxin (30 nM). Iberiotoxin induced vasoconstriction in arteries isolated from both WT and *5x-FAD* mice. However, the vasoconstriction was significantly smaller in *5x-FAD* female mice (Figures 2A and 2B). We corroborated these findings by recording pial artery smooth muscle cell single channel BK_{Ca} currents in an inside-out patch-clamp configuration. We observed an approximately 50% reduction in BK_{Ca} open probability (Po) at -60 mV in patches from *5x-FAD* female mice than those from WT smooth muscle cells (Figures 2C and 2D). This difference was not observed at -40 and -20 mV, when BK_{Ca} Po was nearly abolished in both groups. Together, these findings that BK_{Ca} function is impaired in pial artery smooth muscle cells from female *5x-FAD* mice.

The lower BK_{Ca} function was not related to a downregulation in the BK_{Ca} channel mRNA expression in pial arteries (Figures 2E and 2F), as these were not different between groups, nor to a change in the intracellular Ca^{2+} transients upstream of BK_{Ca} (Figures 2G and 2H). We observed that the frequency of Ca^{2+} transients and the number of active sites per cell were not significantly different between WT and *5x-FAD* mice (Figure 2G). Lastly, mRNA expression of BKα and BKβ subunits in whole brain homogenates were not different between WT and 5x-FAD females (SI Appendix, Figure S5A, and S5B).

Nitro-oxidative stress in 5x-FAD

AD is associated with oxidative stress and inflammation that can contribute to vascular and neuronal damage (33, 42). Thus, we investigated if nitro-oxidative stress was present in the brain of *5x-FAD* females. We observed that the concentration of total glutathione (Figure 3A) and free reduced glutathione (GSH, Figure 3B) were not different between WT and *5x-FAD*. However, there was a significant increase in the amount of oxidized glutathione (GSSG, Figure 3C), resulting in a higher ratio of oxidized glutathione / total glutathione in the brain of female *5x-FAD* when compared to WT littermates (Figure 3D), which suggests a pro-oxidative environment.

The inducible nitric oxide synthase (iNOS) isoform is a pro-inflammatory marker that is increased in AD (43, 44). This isoform produces a high amount of NO, which can lead to nitro-

oxidative damage to cellular structures (45, 46), including excessive nitrosylation of target proteins. Thus, we investigated if iNOS expression is increased in the pial arteries of *5x-FAD* females. Using qPCR, we observed that the expression of iNOS mRNA was increased in the pial arteries from female *5x-FAD* mice compared to WT (Figure 3E). No significant differences were observed for endothelial (eNOS, Figure 3F) or neuronal NOS (nNOS, Figure 3G) in homogenates of pial arteries. Similarly, the fluorescence intensity of iNOS immunolabeling was significantly higher in pial vessels from *5x-FAD* than in WT mice (Figure 3I and 3J). In addition, the non-selective NOS inhibitor L-NAME (200 μM) has a vasoconstrictor effect on PComA from *5x-FAD* females but not in WT, suggesting an upregulation in NO-dependent regulation of basal myogenic tone in these mice (Figure 3H). These results suggest that iNOS is upregulated on the pial vessels, including PComA, in female *5x-FAD* mice.

In addition, *5x-FAD* female mice showed a significantly higher level of S-nitrosylated proteins (S-NO-proteins) in the brain (Figures 3K and 3L) and pial arteries (Figures 3M and 3N) when compared to WT females. Together, these findings suggest there is a nitro-oxidative environment on the brain and pial arteries of *5x-FAD* female mice.

Exarcebation in BK_{Ca} channel S-NO is associated with lower iberiotoxin effect on PComA from female 5x-FAD

BK_{Ca} can undergo S-NO in a nitro-oxidative environment (28); thus, we assessed whether the levels of S-NO BK_{Ca} were increased in female *5x-FAD* using a pull-down assay followed by Western blot. We observed an increase in the amount of S-NO BK_{Ca} in the brain of *5x-FAD* females compared to the WT (Figures 4A and 4B). Moreover, colocalization analyses of immunofluorescence images for S-nitrosylated proteins and BKα subunit (representative fluorogram in Figure 4C, right-side panels) showed that *5x-FAD* pial arteries have higher Manders' M1 (percentage of immunolabeled S-nitrosylated proteins that co-localize with BKα, Figure 4D) and M2 (percentage of immunolabeled BKα that co-localize with S-nitrosylated proteins, Figure 4E) coefficients. Similarly, Pearson's colocalization coefficients were higher in the pial arteries of *5x-FAD* females when compared to WT (Figure 4F). Together, these findings suggest that a higher level of S-NO on BK_{Ca} channels could underlie the reduction in channel activity observed in pressurized PComA experiments. Supporting this hypothesis, pre-incubation of PComA with the reducing agent dithiothreitol (DTT, 10 μM) partially restored iberiotoxin-induced contraction effects in the PComA from *5x-FAD* females mice (Figures 4G and 4H).

Impaired functional neurovascular responses in female 5x-FAD mice

We recently showed that BK_{Ca} dysfunction in cerebral parenchymal arterioles was linked to a reduction in functional vasodilation in the brain of menopausal females (47). Therefore, we rationalize that the blunted BK_{Ca} activity observed in *5x-FAD* females would translate to a lower amplitude of functional hyperemia after somatosensory stimulation. We assessed functional hyperemia responses after somatosensory stimulation by real-time recording of perfusion atop the whisker barrel cortex during mechanical stimulation of contralateral whiskers (47). Under this paradigm, hyperemic responses were blunted in *5x-FAD* females compared to WT littermates (Figures 5A and 5B). These results suggest that 5-month-old female *5x-FAD* mice presented microvascular dysfunction that compromised the brain perfusion and neurovascular reactivity.

Female 5x-FAD mice build incomplete nests

Nest building is an essential activity for rodents, and assessing their ability to build complete nests measures executive function and problem-solving (48). We observed that female *5x-FAD* mice are unable to build complete nests, whereas most nests built by WT mice were nearly complete (Figures 5C and 5D).

Discussion

Our findings suggest a potentially critical mechanism that regulates BK_{Ca} channel function in pial arteries of female *5x-FAD* mice, a model of familial AD. We observed that BK_{Ca} dysfunction likely underlies increased myogenic tone of PComA, leading to reduced perfusion to the frontal cortex as well as blunted functional hyperemia responses. The reduced BK_{Ca} activity is associated with increased S-NO of the pore-forming BKα subunit, a consequence of nitro-oxidative stress resulting from increased iNOS expression and oxidative free radical accumulation in the brain. Our data highlight a novel mechanism by which the nitro-oxidative milieu in the brain of AD subjects affects cerebral microvascular function.

AD is a progressive neurodegenerative disease that disproportionately affects women (49). AD pathology is characterized by neurofibrillary tangles and accumulation of amyloid-β, particularly in the temporal lobe and neocortical structures (50). These alterations are associated with the loss of neuronal synapses and cerebral amyloid angiopathy, which leads to cognitive

deficits (36). Although much focus has been given to the effects of AD pathology on neuronal survival and connectivity, less is known about the mechanisms underlying microvascular dysfunction in the development and progression of AD. Rodents do not develop sporadic AD (51); therefore, the use of transgenic models expressing mutated variants of human amyloid-β precursor protein and presenilin-1 is essential. Specifically, the *5x-FAD* transgenic mouse model combines 3 mutations in the human amyloid precursor protein gene and 2 mutations in the presenilin-1 gene, leading to an accelerated and more aggressive amyloid-β accumulation than other models, resulting in an earlier onset of classical cognitive and histopathological hallmarks (50, 51). Further, the *5x-FAD* mouse is one of the new models of AD that shows significant neuronal loss (52, 53).

Interestingly, there seems to be a significant sex difference in the AD pathology in *5x-FAD*, with females showing higher amyloid-β accumulation than males, as demonstrated by our data and corroborated by others (54). Despite these sex differences in cortical amyloid-β accumulation, we observed that perivascular amyloid-β accumulation in pial arteries is similar between female and male *5x-FAD* mice (re-analysis of data originally published in (37)). Independently of a similar perivascular amyloid-β burden, our data show that the cerebral microvasculature of female *5x-FAD* mice is more susceptible to the deleterious effects of cerebral amyloid angiopathy than that of males.

Using a multi-parametric neuroimaging analysis of the brain from AD patients, Huang *et al.* suggested that cerebral perfusion insufficiency and cortical atrophy could be related to different clinical outcomes in AD patients (55). Since vascular reactivity can directly interfere with baseline cortical perfusion, we performed functional studies on the PComA. This pial arteriole connects the superior cerebellar artery to the circle of Willis. The PComA is an arteriole-sized pial artery (inner diameter < 100 μm) with few or no branches, thus ideal for *ex vivo* pressure myography experiments. Our data showed that PComA from female *5x-FAD* exhibited higher spontaneous myogenic tone than WT littermates, without changes in contractility to 60 mM KCl. As increased myogenic tone can lead to hypoperfusion, as observed in the frontal cortex in female *5x-FAD* mice, we sought to investigate the mechanism involved in this spontaneous hypercontractility in females. Myogenic tone is the result of an equilibrium between depolarizing stimuli (opening of stretch-sensitive cationic channels and voltage-gated Ca^{2+} channels) and hyperpolarizing currents that provide a negative feedback to maintain membrane potential stable in vascular smooth muscle cells, allowing for a sustained and physiological contraction (56). Hyperpolarizing

currents in vascular smooth muscle cells are a consequence of K^+ efflux through K^+- permeable channels, of which BK_{Ca} is a vital component (14).

Impairment in BK_{Ca} function is associated with vascular dysfunction in various disease models, including diabetes (57, 58), hypertension (59), menopause (47, 60), cigarette smoking (61) and, recently, in AD (35). Our findings to this growing body of evidence that smooth muscle BKCa dysfunction contributes to vascular impairments observed in AD. Our data shows that BKCa activity is reduced in pial artery smooth muscle cells, observed as a lower single channel BKCa Po and blunted constriction to iberiotoxin, without changes in mRNA expression or intracellular Ca^{2+} transients. Similar findings were reported by Taylor *et al.* in aged APP23 mice, although, in their study, BK_{Ca} impairment was linked to a reduction in intracellular Ca^{2+} sparks rather than PTMs. The reasons underlying these mechanistic discrepancies are not entirely clear; however, it is possible that the age and different mouse model used in the studies could explain this apparent contradiction. The studies by Taylor *et al.* used APP23 mice at 17 to 19 months-old, whereas we used 5-month-old *5x-FAD* mice. Regardless, the lack of differences in mRNA expression and intracellular Ca^{2+} transients suggest that, in female *5x-FAD* mice, another molecular mechanism underlies BK_{Ca} dysfunction, such as PTMs resulting from nitro-oxidative stress.

Inflammatory responses, systemic and local, have been hypothesized to play a central role in AD and other dementias (42, 62). Early in AD pathogenesis, immune responses result in the clearance of amyloid-β and have an overall protective effect on AD-related brain damage (63, 64). However, prolonged microglia activation can exacerbate AD pathology (62), with sustained pro-inflammatory cytokine signaling resulting in damage to neurons and microglial dysfunction (65-67). Although inflammation is a marker of AD, how this pro-inflammatory environment affects vascular function in AD models remains poorly understood. In our study, we observed an increase in the *5x-FAD* pial artery iNOS expression, both by qPCR and semi-quantitative immunofluorescence. iNOS is mainly expressed in response to a pro-inflammatory stimulus (43), and, differently from the other NOS isoforms, it is effectively locked in an active position due to the tight binding of calmodulin (43, 68), leading to sustained basal NO production. Together with oxidative stress, the higher NO production can result in deleterious S-NO of proteins, as we observed in female *5x-FAD* mice. S-NO is a NO-dependent PTM that consists of the addition of a NO group to a reactive thiol to form an S-nitrosoprotein, regulating protein conformation, protein-protein interactions, and activity (29, 31, 69). In pathological conditions, aberrant S-NO can exacerbate protein dysfunction and contribute to lipid peroxidation, protein nitration, and an

overall nitro-oxidative environment (24, 29, 32, 45, 62, 70-72). Here, we observed that the combination of a nitro-oxidative environment, characterized by iNOS expression and oxidative stress, is associated with increased S-nitrosylation of proteins in the brain of *5x-FAD* females, including BKα.

PTMs are the result of the binding of different moieties to proteins that have a profound effect on their function. They can range from phosphorylation, acetylation, and lipidation to oxidation and nitrosylation (31, 73). PTMs play a vital role in the known heterogeneity and tissue specificity of the biophysical properties of BK_{Ca}, as they have profound effects on gating, voltage and Ca^{2+} sensitivity, and membrane availability of the channel (15). However, how S-NO affects BK_{Ca} remains controversial; some studies show that NO can, directly and indirectly, activate BK_{Ca} (74, 75), whereas others show that NO itself, or peroxynitrite, can blunt BK_{Ca} activity. For instance, a NO-donor failed to activate the BK_{Ca} channel in a heterologous expression system (76). Moreover, Liu *et al.* showed that peroxynitrite reduces the open-state probability of BK_{Ca} channels in isolated vascular smooth muscle cells (70). This finding could explain our observed reduction in BK_{Ca} function in PComA from female *5x-FAD* mice linked to increased BKα S-NO. Further, Lang *et al.* reported that DTT can activate BK_{Ca} (24), likely by reducing previously oxidized thiol groups. Again, this finding supports our observed improvement in BK_{Ca} function after incubation of PComA from *5x-FAD* with DTT. Together, our data highlight a novel molecular mechanism by which the nitro-oxidative environment present in AD brains can lead to microvascular dysfunction by impairing BK_{Ca}.

Ultimately, our observed microvascular dysfunction may underlie the perfusion deficits observed in the brain of *5x-FAD* females. Performing a robust regional assessment of cortical perfusion by laser speckle contrast imaging, we report that female *5x-FAD* mice show reduced basal perfusion to the frontal cortex. In addition, functional hyperemia responses resulting from somatosensory stimulation were also blunted in female *5x-FAD* mice. We recently reported a similar finding in menopausal WT females, where cerebral microvascular BK_{Ca} dysfunction increased myogenic tone and impaired neurovascular coupling (47). Together, these findings suggest that BK_{Ca} may be a master switch for functional vasodilatory responses in the cerebral microcirculation, and its dysfunction may lead to pathological consequences such as cognitive impairment. In support of this possibility, we observed that female *5x-FAD* mice cannot build proper nests. Nest-building behavior involves the coordination of different areas of the brain, including the frontal cortex (48, 77-80). Interestingly, we did not observe deficits in basal perfusion in male *5x-FAD* mice, but they were also incapable of building complete nests. This finding further

highlights the sex differences in the AD pathology and cognitive decline in *5x-FAD*: while it seems that in females, neurovascular dysfunction is central, other pathological mechanisms, yet unidentified, are at play in males.

Conclusion

In conclusion, our results showed that the upregulation of iNOS/RNOS/BK_{Ca} signaling contributes to cerebral microvascular impairments in female *5x-FAD* mice. This vascular dysfunction was associated with reduced basal cortical perfusion to the frontal cortex and blunted neurovascular coupling responses. Our findings suggest that regulating the nitro-oxidative stress can restore the BK_{Ca} function and may improve cerebral microvascular function in AD.

Limitations of the work

We would like to point out one main limitations of our work. We could not perform a direct quantitative assessment of protein expression or PTMs in pial arteries due to the small amount of tissue obtained per mouse. We would need to make pool arteries from at least 5 mice per sample to perform the immunoblotting experiments. Thus, we opted to perform a semi-quantitative analysis using immunofluorescence labeling of the targets of interest (iNOS / BK_{Ca}) only on the pial arteries. To support these analyses, we also performed qPCR on the pial arteries and a Western blot on brain homogenates. Therefore, our functional and molecular data, combined with previous studies in the literature, support our hypotheses and conclusion.

Methods

All animal procedures in this study were approved by the Institutional Animal Care and Use Committee of the University of Arizona College of Medicine (IACUC protocol 18-473) and are in accordance with the National Institutes of Health's Guide for the Care and Use of Laboratory Animals, 8th edition. All animal experiments are reported in compliance with ARRIVE guidelines. The *5x-FAD* mice (5months-old, male and female) used in this study are a transgenic model of early-onset AD that combines five different mutations in two genes associated with Familial AD. Three of the mutations are located in the gene that codes human amyloid precursor protein:

Swedish (K670N, M671L), Florida (I716V), and London (V717I). The other two mutations are inserted in the gene of human presenilin, M146L and L286V. Transgene expression is controlled by the neuronal-specific *Thy1* promoter (52). All mice were bred on a C57bl/6J background, and wild-type (WT) littermates were used as controls. Following euthanasia, the brain was collected and the PComA or remaining pial arteries were dissected. The brain was either fixed in 4% paraformaldehyde for imunofluorescence (confocal microscopy), or flash-frozen for molecular biology experiments (oxidized glutathione assay, protein S-NO, pull-down followed by Western blot and qPCR). A cohort of pial arteries were used for patch-clamp electrophysiology experiments of freshly-isolated smooth muscle cells (single channel BK_{Ca} currents); a separate cohort for spinning disk confocal microscopy to assess intracellular Ca^{2+} transients, and yet another cohort for qPCR. PComA reactivity and structure were studied using pressure myography. Pial arteries were used for qPCR analyses. Baseline cortical perfusion and functional hyperemia following somatosensory stimulation were measured by laser speckle contrasting imaging system. The complete and detailed methodology can be found in the *Supporting Information Appendix - Methodology*.

Acknowledgments

We thank Patricia Jansma, co-manager of the Office Research, Innovation & Impact's Imaging Cores - Optical Facility at the University of Arizona, for providing training service at the microscope and helping with the microscopy image acquisition. We would further like to thank Dr. Anne M. Dorrance (Michigan State University) for her critical review of our manuscript.

Funding Support

This work was supported by the National Institutes of Health (R00 HL140106, R01 AG073230 to PWP), the Alzheimer's Association (AARGD-21-850835 to PWP), and the Arizona Alzheimer's Consortium, Arizona Department of Health Services.

Conflict of interest

The authors declare no conflicts of interest.

Data availability

All data files are stored in the corresponding author's laboratory and are available upon reasonable request.

Author Contribution

JFS – conceived, designed, performed the experiments, analyzed data, and wrote the initial draft of the manuscript;

FDP – performed experiments and analyzed data;

AS – performed the experiments and analyzed data;

MTG – performed the experiments and analyzed data;

AMK – performed experiments and analyzed data;

PWP – conceived, designed, performed experiments, analyzed data and revised the draft of the manuscript.

All authors declare that they reviewed and edited the manuscript, and agree to its submission.

References

1. Anonymous (2021) 2021 Alzheimer's disease facts and figures. *Alzheimers Dement* 17(3):327-406.
2. Girard SD*, et al.* (2013) Evidence for early cognitive impairment related to frontal cortex in the 5XFAD mouse model of Alzheimer's disease. *J Alzheimers Dis* 33(3):781-796.
3. Collaborators GBDDF (2022) Estimation of the global prevalence of dementia in 2019 and forecasted prevalence in 2050: an analysis for the Global Burden of Disease Study 2019. *Lancet Public Health* 7(2):e105-e125.
4. Salloway S*, et al.* (2014) Two phase 3 trials of bapineuzumab in mild-to-moderate Alzheimer's disease. *N Engl J Med* 370(4):322-333.
5. Jellinger KA (2002) Alzheimer disease and cerebrovascular pathology: an update. *J Neural Transm (Vienna)* 109(5-6):813-836.
6. Mehndiratta P*, et al.* (2012) Cerebral amyloid angiopathy-associated intracerebral hemorrhage: pathology and management. *Neurosurg Focus* 32(4):E7.

7. Gireud-Goss M, Mack AF, McCullough LD, & Urayama A (2021) Cerebral Amyloid Angiopathy and Blood-Brain Barrier Dysfunction. *Neuroscientist* 27(6):668-684.
8. Greenberg SM, Gurol ME, Rosand J, & Smith EE (2004) Amyloid angiopathy-related vascular cognitive impairment. *Stroke* 35(11 Suppl 1):2616-2619.
9. Shin HK*, et al.* (2007) Age-dependent cerebrovascular dysfunction in a transgenic mouse model of cerebral amyloid angiopathy. *Brain* 130(Pt 9):2310-2319.
10. Iadecola C (2017) The Neurovascular Unit Coming of Age: A Journey through Neurovascular Coupling in Health and Disease. *Neuron* 96(1):17-42.
11. Nelson MT & Quayle JM (1995) Physiological roles and properties of potassium channels in arterial smooth muscle. *Am J Physiol* 268(4 Pt 1):C799-822.
12. Brenner R*, et al.* (2000) Vasoregulation by the beta1 subunit of the calcium-activated potassium channel. *Nature* 407(6806):870-876.
13. Jaggar JH, Porter VA, Lederer WJ, & Nelson MT (2000) Calcium sparks in smooth muscle. *Am J Physiol Cell Physiol* 278(2):C235-256.
14. Krishnamoorthy-Natarajan G & Koide M (2016) BK Channels in the Vascular System. *Int Rev Neurobiol* 128:401-438.
15. Kyle BD & Braun AP (2014) The regulation of BK channel activity by pre- and post-translational modifications. *Front Physiol* 5:316.
16. Tian L*, et al.* (2008) Palmitoylation gates phosphorylation-dependent regulation of BK potassium channels. *Proc Natl Acad Sci U S A* 105(52):21006-21011.
17. Schubert R & Nelson MT (2001) Protein kinases: tuners of the BKCa channel in smooth muscle. *Trends Pharmacol Sci* 22(10):505-512.
18. Munzel T*, et al.* (2003) Physiology and pathophysiology of vascular signaling controlled by guanosine 3',5'-cyclic monophosphate-dependent protein kinase [corrected]. *Circulation* 108(18):2172-2183.
19. Kyle BD, Hurst S, Swayze RD, Sheng J, & Braun AP (2013) Specific phosphorylation sites underlie the stimulation of a large conductance, Ca(2+)-activated K(+) channel by cGMP-dependent protein kinase. *FASEB J* 27(5):2027-2038.
20. Nara M, Dhulipala PD, Wang YX, & Kotlikoff MI (1998) Reconstitution of beta-adrenergic modulation of large conductance, calcium-activated potassium (maxi-K) channels in Xenopus oocytes. Identification of the camp-dependent protein kinase phosphorylation site. *J Biol Chem* 273(24):14920-14924.

21. Lin MT, Hessinger DA, Pearce WJ, & Longo LD (2006) Modulation of BK channel calcium affinity by differential phosphorylation in developing ovine basilar artery myocytes. *Am J Physiol Heart Circ Physiol* 291(2):H732-740.
22. Zhou XB*, et al.* (2010) Dual role of protein kinase C on BK channel regulation. *Proc Natl Acad Sci U S A* 107(17):8005-8010.
23. Thuringer D & Findlay I (1997) Contrasting effects of intracellular redox couples on the regulation of maxi-K channels in isolated myocytes from rabbit pulmonary artery. *J Physiol* 500 (Pt 3)(Pt 3):583-592.
24. Lang RJ, Harvey JR, McPhee GJ, & Klemm MF (2000) Nitric oxide and thiol reagent modulation of Ca2+-activated K+ (BKCa) channels in myocytes of the guinea-pig taenia caeci. *J Physiol* 525 Pt 2(Pt 2):363-376.
25. Brzezinska AK, Gebremedhin D, Chilian WM, Kalyanaraman B, & Elliott SJ (2000) Peroxynitrite reversibly inhibits Ca(2+)-activated K(+) channels in rat cerebral artery smooth muscle cells. *Am J Physiol Heart Circ Physiol* 278(6):H1883-1890.
26. Wang ZW, Nara M, Wang YX, & Kotlikoff MI (1997) Redox regulation of large conductance Ca(2+)-activated K+ channels in smooth muscle cells. *J Gen Physiol* 110(1):35-44.
27. Soto MA, Gonzalez C, Lissi E, Vergara C, & Latorre R (2002) Ca(2+)-activated K+ channel inhibition by reactive oxygen species. *Am J Physiol Cell Physiol* 282(3):C461-471.
28. Tang XD, Garcia ML, Heinemann SH, & Hoshi T (2004) Reactive oxygen species impair Slo1 BK channel function by altering cysteine-mediated calcium sensing. *Nat Struct Mol Biol* 11(2):171-178.
29. Furuta S (2017) Basal S-Nitrosylation Is the Guardian of Tissue Homeostasis. *Trends Cancer* 3(11):744-748.
30. Butterfield DA & Boyd-Kimball D (2020) Mitochondrial Oxidative and Nitrosative Stress and Alzheimer Disease. *Antioxidants (Basel)* 9(9).
31. Handy DE & Loscalzo J (2006) Nitric oxide and posttranslational modification of the vascular proteome: S-nitrosation of reactive thiols. *Arterioscler Thromb Vasc Biol* 26(6):1207-1214.
32. Su B*, et al.* (2008) Oxidative stress signaling in Alzheimer's disease. *Curr Alzheimer Res* 5(6):525-532.
33. Asiimwe N, Yeo SG, Kim MS, Jung J, & Jeong NY (2016) Nitric Oxide: Exploring the Contextual Link with Alzheimer's Disease. *Oxid Med Cell Longev* 2016:7205747.

34. Girouard H, Park L, Anrather J, Zhou P, & Iadecola C (2007) Cerebrovascular nitrosative stress mediates neurovascular and endothelial dysfunction induced by angiotensin II. *Arterioscler Thromb Vasc Biol* 27(2):303-309.
35. Taylor JL*, et al.* (2022) Functionally linked potassium channel activity in cerebral endothelial and smooth muscle cells is compromised in Alzheimer's disease. *Proc Natl Acad Sci U S A* 119(26):e2204581119.
36. Anonymous (2022) 2022 Alzheimer's disease facts and figures. *Alzheimers Dement* 18(4):700-789.
37. Peters EC*, et al.* (2022) Amyloid-beta disrupts unitary calcium entry through endothelial NMDA receptors in mouse cerebral arteries. *J Cereb Blood Flow Metab* 42(1):145-161.
38. Polycarpou A*, et al.* (2016) Adaptation of the cerebrocortical circulation to carotid artery occlusion involves blood flow redistribution between cortical regions and is independent of eNOS. *Am J Physiol Heart Circ Physiol* 311(4):H972-H980.
39. Jackson WF (2021) Myogenic Tone in Peripheral Resistance Arteries and Arterioles: The Pressure Is On! *Front Physiol* 12:699517.
40. Claassen J, Thijssen DHJ, Panerai RB, & Faraci FM (2021) Regulation of cerebral blood flow in humans: physiology and clinical implications of autoregulation. *Physiol Rev* 101(4):1487-1559.
41. Wang S*, et al.* (2022) Impact of impaired cerebral blood flow autoregulation on cognitive impairment. *Front Aging* 3:1077302.
42. Newcombe EA*, et al.* (2018) Inflammation: the link between comorbidities, genetics, and Alzheimer's disease. *J Neuroinflammation* 15(1):276.
43. Cinelli MA, Do HT, Miley GP, & Silverman RB (2020) Inducible nitric oxide synthase: Regulation, structure, and inhibition. *Med Res Rev* 40(1):158-189.
44. Kleinert H, Schwarz PM, & Forstermann U (2003) Regulation of the expression of inducible nitric oxide synthase. *Biol Chem* 384(10-11):1343-1364.
45. Forstermann U, Xia N, & Li H (2017) Roles of Vascular Oxidative Stress and Nitric Oxide in the Pathogenesis of Atherosclerosis. *Circ Res* 120(4):713-735.
46. Weidinger A*, et al.* (2015) Vicious inducible nitric oxide synthase-mitochondrial reactive oxygen species cycle accelerates inflammatory response and causes liver injury in rats. *Antioxid Redox Signal* 22(7):572-586.
47. Blackwell JA*, et al.* (2022) Cerebral arteriolar and neurovascular dysfunction after chemically induced menopause in mice. *Am J Physiol Heart Circ Physiol* 323(5):H845-H860.

48. Deacon RM (2006) Assessing nest building in mice. *Nat Protoc* 1(3):1117-1119.
49. Mielke MM (2018) Sex and Gender Differences in Alzheimer's Disease Dementia. *Psychiatr Times* 35(11):14-17.
50. Breijyeh Z & Karaman R (2020) Comprehensive Review on Alzheimer's Disease: Causes and Treatment. *Molecules* 25(24).
51. Esquerda-Canals G, Montoliu-Gaya L, Guell-Bosch J, & Villegas S (2017) Mouse Models of Alzheimer's Disease. *J Alzheimers Dis* 57(4):1171-1183.
52. Oakley H*, et al.* (2006) Intraneuronal beta-amyloid aggregates, neurodegeneration, and neuron loss in transgenic mice with five familial Alzheimer's disease mutations: potential factors in amyloid plaque formation. *J Neurosci* 26(40):10129-10140.
53. Eimer WA & Vassar R (2013) Neuron loss in the 5XFAD mouse model of Alzheimer's disease correlates with intraneuronal Abeta42 accumulation and Caspase-3 activation. *Mol Neurodegener* 8:2.
54. Forner S*, et al.* (2021) Systematic phenotyping and characterization of the 5xFAD mouse model of Alzheimer's disease. *Sci Data* 8(1):270.
55. Huang CW*, et al.* (2018) Cerebral Perfusion Insufficiency and Relationships with Cognitive Deficits in Alzheimer's Disease: A Multiparametric Neuroimaging Study. *Sci Rep* 8(1):1541.
56. Jackson WF (2021) Calcium-Dependent Ion Channels and the Regulation of Arteriolar Myogenic Tone. *Front Physiol* 12:770450.
57. Nieves-Cintron M*, et al.* (2017) Impaired BK(Ca) channel function in native vascular smooth muscle from humans with type 2 diabetes. *Sci Rep* 7(1):14058.
58. Lu T*, et al.* (2019) Downregulation of BK channel function and protein expression in coronary arteriolar smooth muscle cells of type 2 diabetic patients. *Cardiovasc Res* 115(1):145-153.
59. Grimm PR & Sansom SC (2010) BK channels and a new form of hypertension. *Kidney Int* 78(10):956-962.
60. Reed JT, Pareek T, Sriramula S, & Pabbidi MR (2020) Aging influences cerebrovascular myogenic reactivity and BK channel function in a sex-specific manner. *Cardiovasc Res* 116(7):1372-1385.
61. Le T*, et al.* (2021) Secondhand Smoke Exposure Impairs Ion Channel Function and Contractility of Mesenteric Arteries. *Function (Oxf)* 2(5):zqab041.
62. Kinney JW*, et al.* (2018) Inflammation as a central mechanism in Alzheimer's disease. *Alzheimers Dement (N Y)* 4:575-590.

63. Shaftel SS*, et al.* (2007) Sustained hippocampal IL-1 beta overexpression mediates chronic neuroinflammation and ameliorates Alzheimer plaque pathology. *J Clin Invest* 117(6):1595-1604.

64. Bolmont T*, et al.* (2008) Dynamics of the microglial/amyloid interaction indicate a role in plaque maintenance. *J Neurosci* 28(16):4283-4292.

65. Hickman SE, Allison EK, & El Khoury J (2008) Microglial dysfunction and defective beta-amyloid clearance pathways in aging Alzheimer's disease mice. *J Neurosci* 28(33):8354-8360.

66. Krabbe G*, et al.* (2013) Functional impairment of microglia coincides with Beta-amyloid deposition in mice with Alzheimer-like pathology. *PLoS One* 8(4):e60921.

67. Sheng JG, Zhou XQ, Mrak RE, & Griffin WS (1998) Progressive neuronal injury associated with amyloid plaque formation in Alzheimer disease. *J Neuropathol Exp Neurol* 57(7):714-717.

68. Venema RC, Sayegh HS, Kent JD, & Harrison DG (1996) Identification, characterization, and comparison of the calmodulin-binding domains of the endothelial and inducible nitric oxide synthases. *J Biol Chem* 271(11):6435-6440.

69. Gupta KJ*, et al.* (2020) Regulating the regulator: nitric oxide control of post-translational modifications. *New Phytol* 227(5):1319-1325.

70. Liu Y*, et al.* (2002) Peroxynitrite inhibits Ca2+-activated K+ channel activity in smooth muscle of human coronary arterioles. *Circ Res* 91(11):1070-1076.

71. Radi R (2018) Oxygen radicals, nitric oxide, and peroxynitrite: Redox pathways in molecular medicine. *Proc Natl Acad Sci U S A* 115(23):5839-5848.

72. Takeda S, Sato N, & Morishita R (2014) Systemic inflammation, blood-brain barrier vulnerability and cognitive/non-cognitive symptoms in Alzheimer disease: relevance to pathogenesis and therapy. *Front Aging Neurosci* 6:171.

73. Liu YP, Zhang TN, Wen R, Liu CF, & Yang N (2022) Role of Posttranslational Modifications of Proteins in Cardiovascular Disease. *Oxid Med Cell Longev* 2022:3137329.

74. Bolotina VM, Najibi S, Palacino JJ, Pagano PJ, & Cohen RA (1994) Nitric oxide directly activates calcium-dependent potassium channels in vascular smooth muscle. *Nature* 368(6474):850-853.

75. Hou S, Heinemann SH, & Hoshi T (2009) Modulation of BKCa channel gating by endogenous signaling molecules. *Physiology (Bethesda)* 24:26-35.

76. Hou S, Xu R, Heinemann SH, & Hoshi T (2008) The RCK1 high-affinity Ca2+ sensor confers carbon monoxide sensitivity to Slo1 BK channels. *Proc Natl Acad Sci U S A* 105(10):4039-4043.

77. Kolb B (1984) Functions of the frontal cortex of the rat: a comparative review. *Brain Res* 320(1):65-98.

78. Alsina-Llanes M & Olazabal DE (2020) Prefrontal cortex is associated with the rapid onset of parental behavior in inexperienced adult mice (C57BL/6). *Behav Brain Res* 385:112556.

79. Corder KM*, et al.* (2018) Prefrontal cortex-dependent innate behaviors are altered by selective knockdown of Gad1 in neuropeptide Y interneurons. *PLoS One* 13(7):e0200809.

80. Filali M & Lalonde R (2009) Age-related cognitive decline and nesting behavior in an APPswe/PS1 bigenic model of Alzheimer's disease. *Brain Res* 1292:93-99.

Figure Legends

Figure 1. *Pronounced AD and cerebral microvascular pathology in female 5x-FAD.* **A)** Representative images of thioflavin-T-stained amyloid-β plaques (bright green) in the cortex (left panels) and dorsal hippocampus (right panels) from female (upper images) and male (lower images) *5x-FAD* mice. Note the higher number of plaques in females. Bar = 200 µm. **B)** Summary data from quantification of amyloid-β plaques. *p<0.05, two-tailed Mann-Whitney test. Each individual data point in the graph represents 1 mouse. **C)** Representative images (left panels) from laser speckle contrast imaging assessment of cortical perfusion in female WT (top) and *5x-FAD* (lower). Quantification is found in the bar graph on the right. FC: frontal cortex; PC: parietal cortex; ZPA: zone of pial anastomoses; TC: temporal cortex; WC: whole cortex. *p<0.05, two-way ANOVA. Each individual data point in graph represents 1 mouse. **D)** Representative images (left panels) from laser speckle contrast imaging assessment of cortical perfusion in male WT (top) and *5x-FAD* (lower). Quantification is found in the bar graph on the right. Each individual data point in graph represents 1 mouse. **E)** Representative traces of the lumen diameter of PComA isolated from WT (black, top) or *5x-FAD* (lower, red) female mice during the generation of spontaneous myogenic tone. **F)** Summary data showing higher spontaneous myogenic tone in the PComA from female *5x-FAD* mice. *p<0.05, two-tailed *Student's* t-test. Each data point in the graph represents 1 PComA from 1 separate mouse. **G)** No differences were observed in vasoconstriction to 60 mM KCl applied to the superfusing bath. H) Endothelium denudation abolished the difference in myogenic tone in PComA from *5x-FAD* females. **I-L)** No differences in PComA contractile reactivity were observed between male WT and *5x-FAD* mice, as observed by similar spontaneous myogenic tone **(I-J)**, constriction to 60 mM KCl **(K),** and myogenic tone after endothelium denudation **(L)**. All data are means ± SEM.

Figure 2. *BK_{Ca} impairment in PComA from female 5x-FAD.* **A)** Representative traces of the lumen diameter of PComA isolated from WT (black, top) or *5x-FAD* (lower, red) female mice showing constriction to the BK_{Ca} blocker iberiotoxin. Note the blunted constriction in *5x-FAD* mice. Orange boxes: regions where data were obtained**.** **B**) Summary bar graph showing blunted vasoconstriction to iberiotoxin in the PComA from female *5x-FAD* mice. Data are means ± SEM, *p<0.05, two-tailed *Student's* t-test. Each data point in the graph represents 1 PComA from 1 separate mouse. **C)** Representative traces of an inside-out patch clamp from pial artery SMC showing single channel BK_{Ca} currents at a holding potential of -60 mV. Note the higher frequency of openings (down-ward deflections) in the patch from WT (top trace, black) compared to the

frequency in *5x-FAD* female mice (lower trace, red). D) Summary graph showing the open probability of BK_{Ca} over a range of holding potentials (-60, -40 and -20 mV). Po was significantly lower in inside-out patches from pial artery smooth muscle cells isolated from female *5x-FAD* mice. *p<0.05, two-way ANOVA with a Sidak post-hoc test. Data are means ± SEM, each data point in the graph represents 1 patch from 3 WT and 2 *5x-FAD* mice. **E-F)** mRNA for the BKα **(E)** and BKβ **(F)** subunits were not different in pial arteries from WT and *5x-FAD*. Data are means ± SEM, and each data point in the graph represents 1 mouse. **G-H)** No differences were observed in smooth muscle cell intracellular Ca^{2+} transients between WT and *5x-FAD* females, as observed in the frequency of events **(G)** and number of active sites per cell **(H)**. The middle line in violin plots represents the mean, and the upper and lower lines are the 95% confidence interval. N = 3 pial arteries from 3 mice per group.

Figure 3. Nitro-oxidative stress in the brain and pial arteries of *5x-FAD* females. **A-D)** Assessment of oxidative stress in the brain of 5x-FAD females via quantification of oxidized glutathione. Total **(A)** and free **(B)** reduced glutathione (GSH) were not different between WT and *5x-FAD*; however, oxidized glutathione (GSSG) was elevated in the brain of female *5x-FAD* **(C)**. Consequently, the GSSG: total GSH ratio was significantly elevated in the brain of female *5x-FAD* mice **(D)**. *p<0.05, two-tailed *Student's* t-test. Each data point in the graph represents 1 mouse. **E)** iNOS mRNA was significantly higher in pial arteries from female *5x-FAD* mice when compared to WT, without changes in eNOS **(F)** or nNOS **(G)**. *p<0.05, two-tailed *Student's* t-test. **H)** NOS inhibition with L-NNA (200 μM) caused a significant contraction of pressurized PComA from female *5x-FAD* mice but not WT, indicating over-activity of the NO pathway in these vessels. **I)** Representative immunofluorescence images labeling for collagen IV (green) and iNOS (red) in pial vessels of WT (top panels) and *5x-FAD* (lower panels). Note the higher fluorescence in pial vessels of *5x-FAD* (lower panels). Bar = 20 μm. **J)** Quantification of iNOS fluorescence intensity. Each data point in the graph corresponds to the average fluorescence intensity of all pial vessels in a region of interest. N = 5 mice per group. *p<0.05, two-tailed *Student's* t-test. **K-L)** Increased protein S-nitrosylation (S-NO) in the brain of female *5x-FAD* mice when compared to WT, as observed in the representative blot **(K)** and the summary bar graph **(L)**. *p<0.05, two-tailed *Student's* t-test, each data point represents 1 mouse. **M-N)** Higher S-NO fluorescence intensity in pial vessels of 5x-FAD, as seen in the representative images **(M)** and summary graph **(N)**. Each data point in the graph corresponds to the average fluorescence intensity of all pial vessels in a region of

interest. N = 5 mice per group. *p<0.05, two-tailed *Student's* t-test. All data in this figure are means ± SEM.

Figure 4. *Increased BK_{Ca} S-NO in female 5x-FAD mice.* **A)** Representative blot of S-NO pull-down assay followed by Western blot against BKα in brain homogenates of female WT and *5x-FAD* mice. **B)** Summary bar graph of the quantification of S-NO BKα. *p<0.05, two-tailed *Student's* t-test, each data point in the graph represents brain homogenates from an individual mouse. Data are means ± SEM. **C)** Representative immunofluorescence images of brain slices from WT (top panels) and *5x-FAD* (lower panels) co-immunolabeled against S-NO proteins (red) and BKα to perform a semi-quantitative colocalization analysis. White arrows indicate the pial vessels analyzed in each image. The fluorogram on the right shows the distribution of co-localized pixels in the images. Bar = 20 μm. **D-F**) Mander's correlation coefficient of colocalization, showing a significant increase in both M1-Mander's coefficient (**D**, S-NO pixels that co-localize with BKα) and M2-Mander's coefficient (**E**, BKα pixels that co-localize with S-NO proteins) in pial vessels from 5x-FAD females when compared to WT controls. Similarly, the Pearson's colocalization coefficient is significantly increased in the pial arteries from female 5x-FAD mice (**F**). *p<0.05, two-tailed Student's t-test. Lines on the violin plot are: thick line = mean, thin lines = 95% confidence intervals. N = 5 randomly selected pial vessels per mouse, a total of 3 mice per group. **G)** Representative trace of the lumen diameter of a pressurized PComA from a female 5x-FAD mouse showing the response to the BKCa inhibitor iberiotoxin (30 nM) before and after incubation with the reducing agent DTT (1 mM). Note that DTT increases the response to iberiotoxin. **H)** Summary data showing that DTT partially restores BKCa in PcomA from female 5x-FAD. *p<0.05, paired two-tailed *Student's* t-test. Each data point represents 1 PcomA from an individual mouse. Data are means ± SEM.

Figure 5. *Neurovascular and cognitive impairment in 5x-FAD females.* **A)** Representative perfusion heatmaps atop the mouse whisker barrel cortex of WT (top panels) and *5x-FAD* (lower panels) before stimulation (left), during stimulation (middle), and after stimulation (left) of the contralateral whiskers. PU = perfusion units. **B)** Summary bar graph showing that functional hyperemia responses are impaired in female *5x-FAD* mice compared to WT littermates. *p<0.05, two-tailed *Student's* t-test. Each data point is the average of 3 consecutive trials in an individual mouse. **C)** Representative images of nests made by WT (left image) and *5x-FAD* (right) females.

Note the incomplete nest in the *5x-FAD* cage. **D)** Summary bar graph of nesting scores showing that female *5x-FAD* mice build significantly incomplete nests. *$p<0.05$, Kolmogorov-Smirnov test. Each data point represents an average of 3 scores from 3 separate investigators blinded to the experimental groups. Data are means ± SEM.

Figure 1. *Sex differences in the 5x-FAD model of AD*

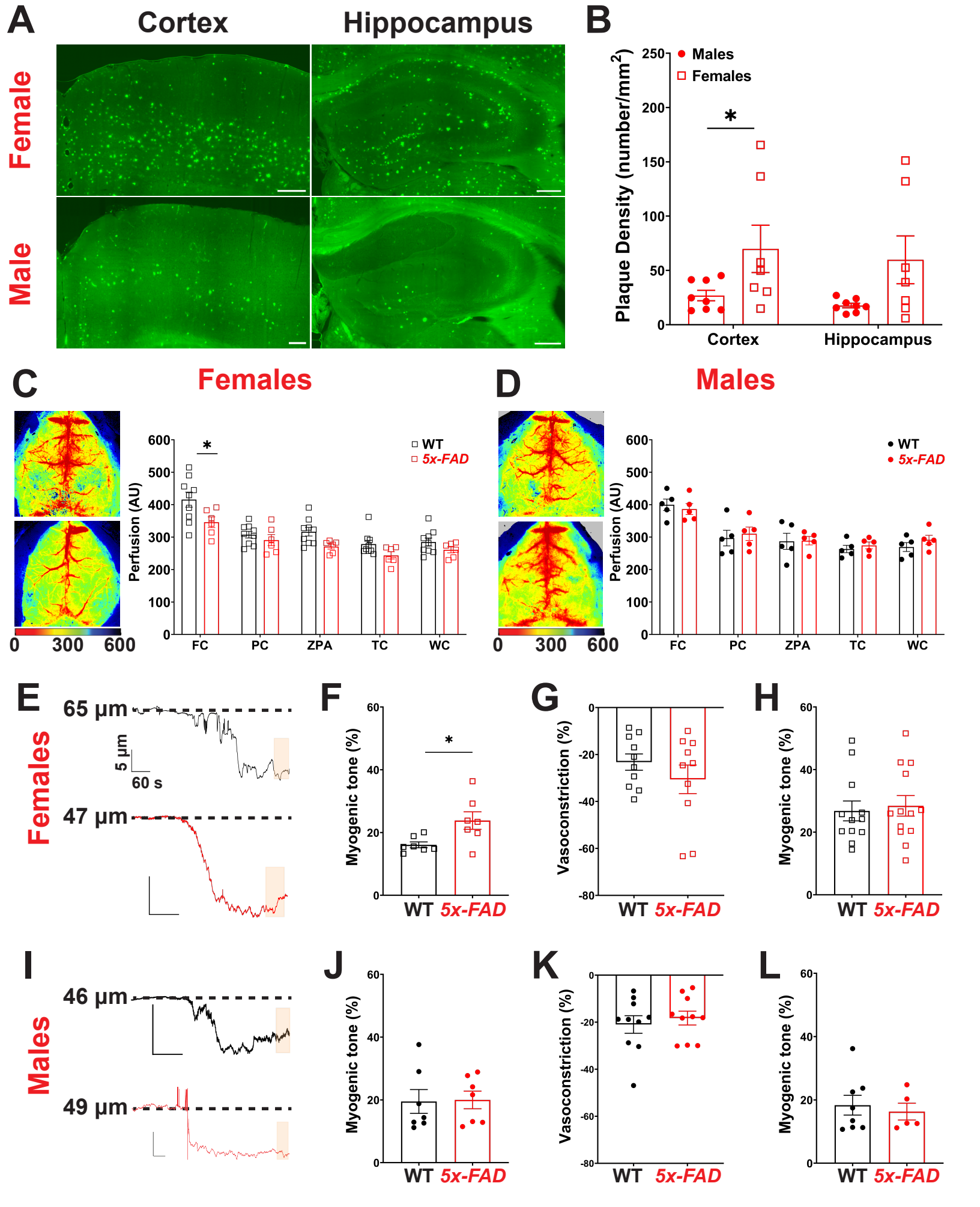

Figure 2. *BK impairment in female 5x-FAD*

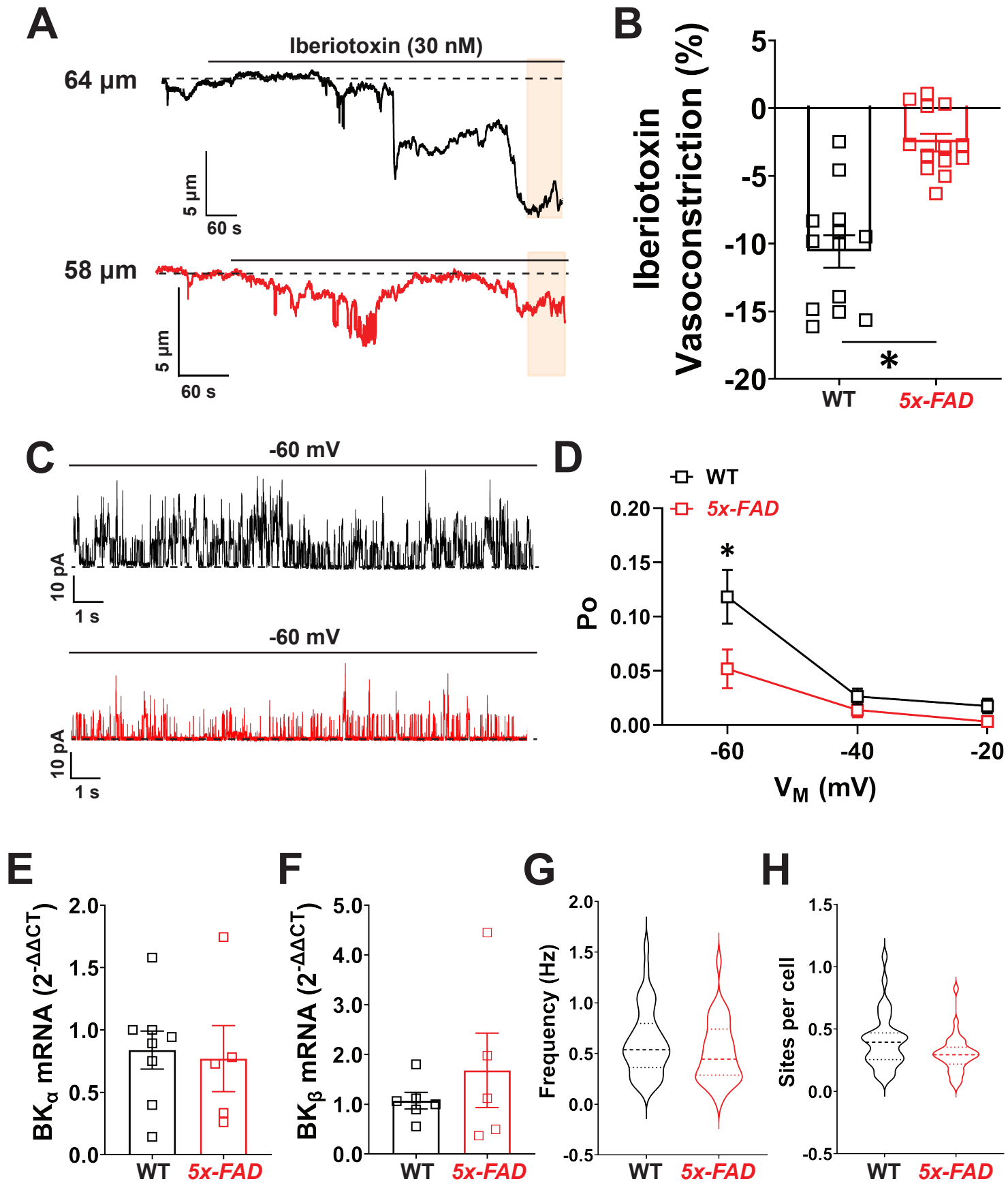

Figure 3. *Nitro-oxidative stress in 5x-FAD females*

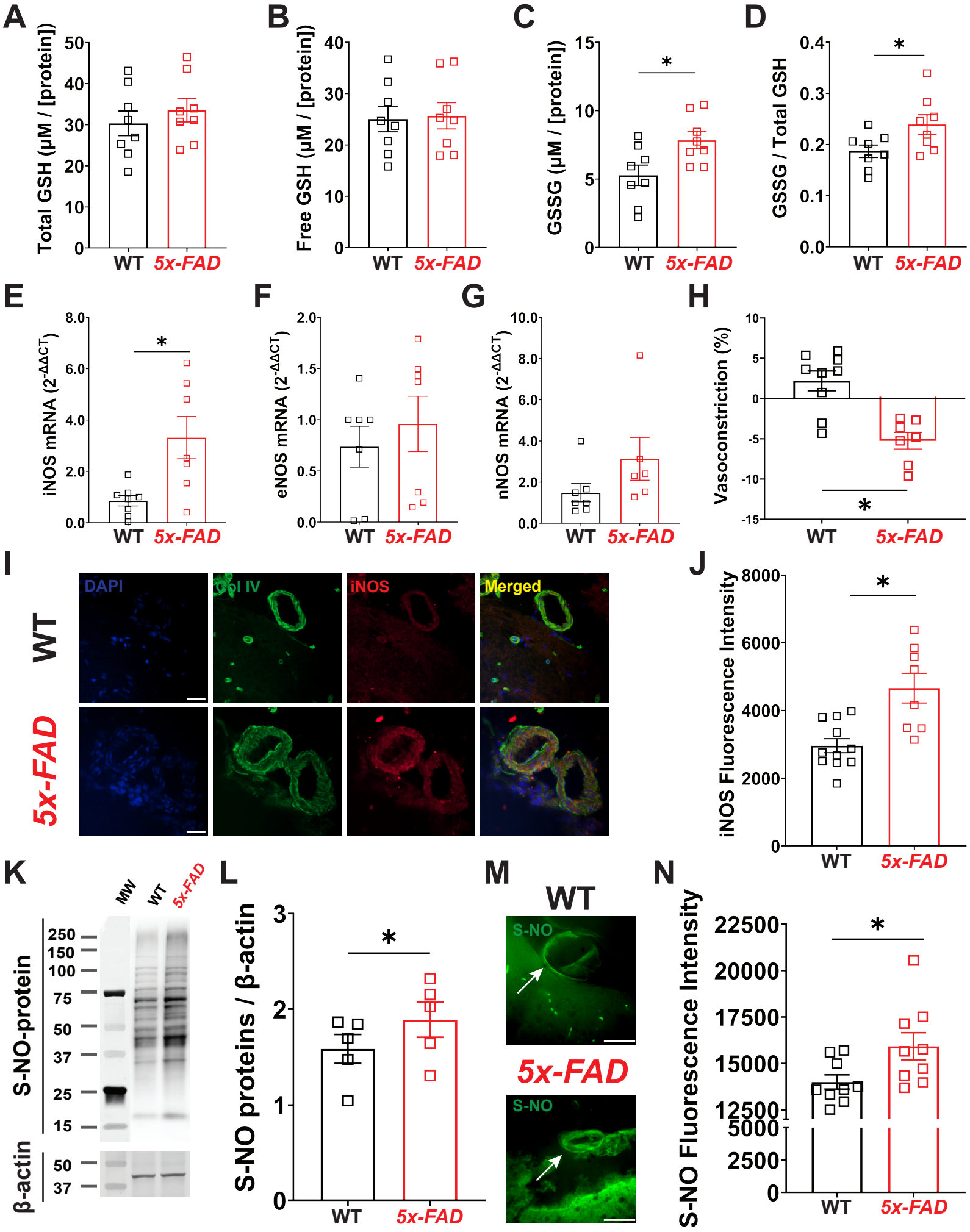

Figure 4. *BK_{Ca} S-nitrosilation in female 5x-FAD*

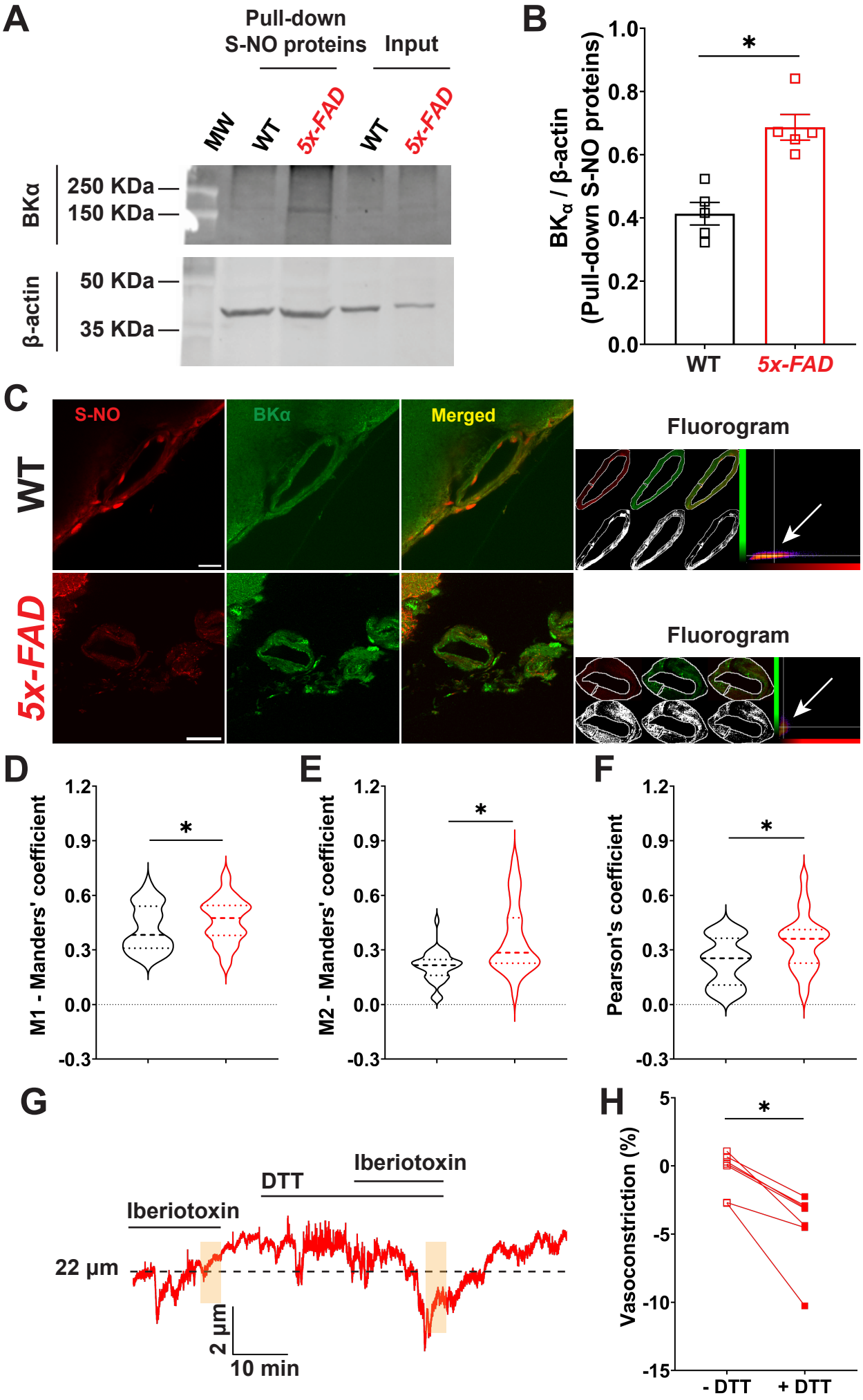
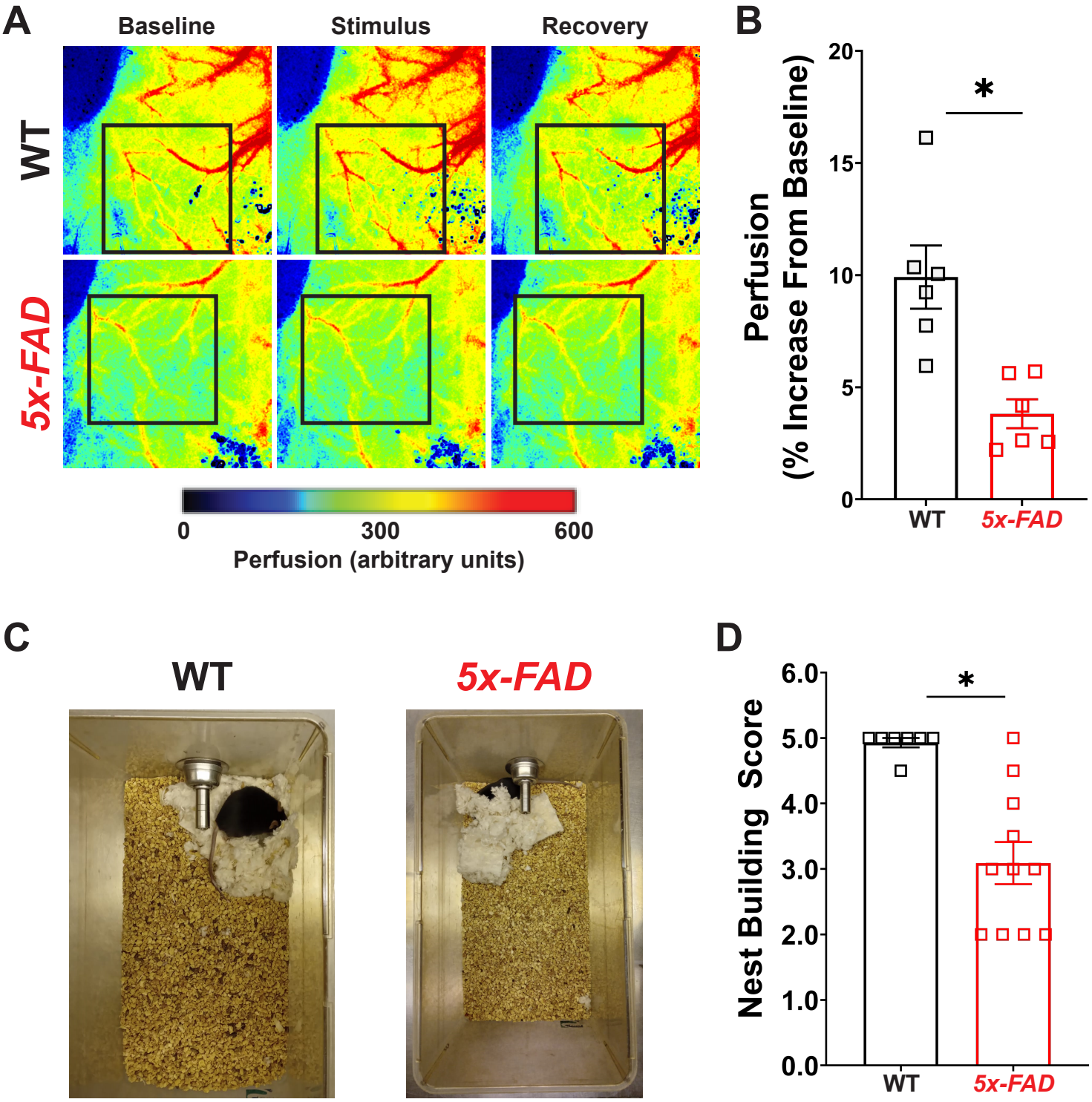
Figure 5. *Neurovascular deficits in female 5x-FAD*